

# Phoretic Liquid Metal Micro/Nanomotors as Intelligent Filler for Targeted Microwelding

Yong Wang, Wendi Duan, Chao Zhou, Qing Liu, Jiahui Gu, Heng Ye, Mingyu Li, Wei Wang,\* and Xing Ma\*

Micro/nanomotors (MNM) have emerged as active micro/nanoplatforms that can move and perform functions at small scales. Much of their success, however, hinges on the use of functional properties of new materials. Liquid metals (LMs), due to their good electrical conductivity, biocompatibility, and flexibility, have attracted considerable attentions in the fields of flexible electronics, biomedicine, and soft robotics. The design and construction of LM-based motors is therefore a research topic with tremendous prospects, however current approaches are mostly limited to macroscales. Here, the fabrication of an LM-MNM (made of Galinstan, a gallium–indium–tin alloy) is reported and its potential application as an on-demand, self-targeting welding filler is demonstrated. These LM-MNMs (as small as a few hundred nanometers) are half-coated with a thin layer of platinum (Pt) and move in  $\text{H}_2\text{O}_2$  via self-electrophoresis. In addition, the LM-MNMs roaming in a silver nanowire network can move along the nanowires and accumulate at the contact junctions where they become fluidic and achieve junction microwelding at room temperature by reacting with acid vapor. This work presents an intelligent and soft nanorobot capable of repairing circuits by welding at small scales, thus extending the pool of available self-propelled MNMs and introducing new applications.

In recent years, there has been growing interest in micro/nanomotors (MNM, also known as colloidal motors or synthetic microswimmers) due to their controlled self-propulsion and on-demand operability at small scales.<sup>[1,2]</sup> In the nearly two decades since their introduction,<sup>[3]</sup> MNMs have demonstrated their exciting potential as autonomous and intelligent micro/nanotools for drug delivery,<sup>[4]</sup> microsurgery,<sup>[5]</sup> biosensing,<sup>[6]</sup> pollutant degradation,<sup>[7]</sup> and many other applications. In addition, MNMs are also widely used in physics as a model system


to study active matter.<sup>[8]</sup> Due to their immense versatility, the material chemistry community has undertaken great efforts to synthesize functional MNMs from different materials with distinctive structures using a range of synthesis and fabrication techniques.<sup>[1,9]</sup> Since the specific range of applications of a particular MNM is inherently linked to its intrinsic material properties, such as being catalytic, magnetic, or photoactive, a great research effort has gone into the pursuit of an ever-expanding selection of materials with unique properties.<sup>[9,10]</sup>

One such group of materials is liquid metals (LMs). Low melting point LMs are fluidic at room temperature while maintaining the same electrical conductivity as regular metals. A fascinating material with unique properties,<sup>[11]</sup> LMs are widely used for printing flexible electronic circuits and sensors<sup>[12]</sup> and have also been utilized in nanomedicine for biomedical theranostics as they are both deformable and biocompatible.<sup>[13]</sup> Several implemen-

tations of LM motors have appeared over the past few years, although typically operating at macroscopic ( $\geq 1$  mm) scales. For example, millimeter-scale LM (Galinstan) motors achieved directional self-propulsion via the Marangoni effect, caused by an imbalance of surface tension arising either from an external electric field<sup>[14]</sup> or pH (or ionic) gradient.<sup>[15]</sup> In another example, millimeter-scale LM (EGaIn and Galinstan) droplets with attached aluminum flakes were shown to move in sodium hydroxide solution by bubble propulsion.<sup>[16]</sup> Moreover, an early study showed that LM (Galinstan) droplets coated with  $\text{WO}_3$  nanoparticles as photocatalysts could be propelled by bubbles via photochemical reactions of  $\text{WO}_3$  with  $\text{H}_2\text{O}_2$ .<sup>[17]</sup> Although these pioneering studies have made great strides in LM-based motors, efforts to downscale them to micro- and nanoscale are still rare. Two particular challenges that LM-MNMs have to overcome are Brownian motion and the highly viscous environment for microscopic swimmers which require different propulsion mechanisms than for macroscopic LM motors. A recent pioneering study fabricated LM microrods using a template method and studied their propulsion via ultrasound as well as their usefulness in biomedical applications such as cancer therapy.<sup>[18]</sup> This opened up tremendous possibilities of using LM-MNMs for a range of applications at micro/nanoscales beyond cancer therapy.

Y. Wang, W. Duan, Q. Liu, J. Gu, Dr. H. Ye, Prof. M. Li, Prof. X. Ma  
State Key Laboratory of Advanced Welding and Joining (Shenzhen) and  
Flexible Printed Electronic Technology Center  
Harbin Institute of Technology (Shenzhen)  
Shenzhen 518055, China  
E-mail: maxing@hit.edu.cn

C. Zhou, Prof. W. Wang  
School of Materials Science and Engineering  
Harbin Institute of Technology (Shenzhen)  
Shenzhen 518055, China  
E-mail: weiwangsz@hit.edu.cn

 The ORCID identification number(s) for the author(s) of this article can be found under <https://doi.org/10.1002/adma.201905067>.

DOI: 10.1002/adma.201905067

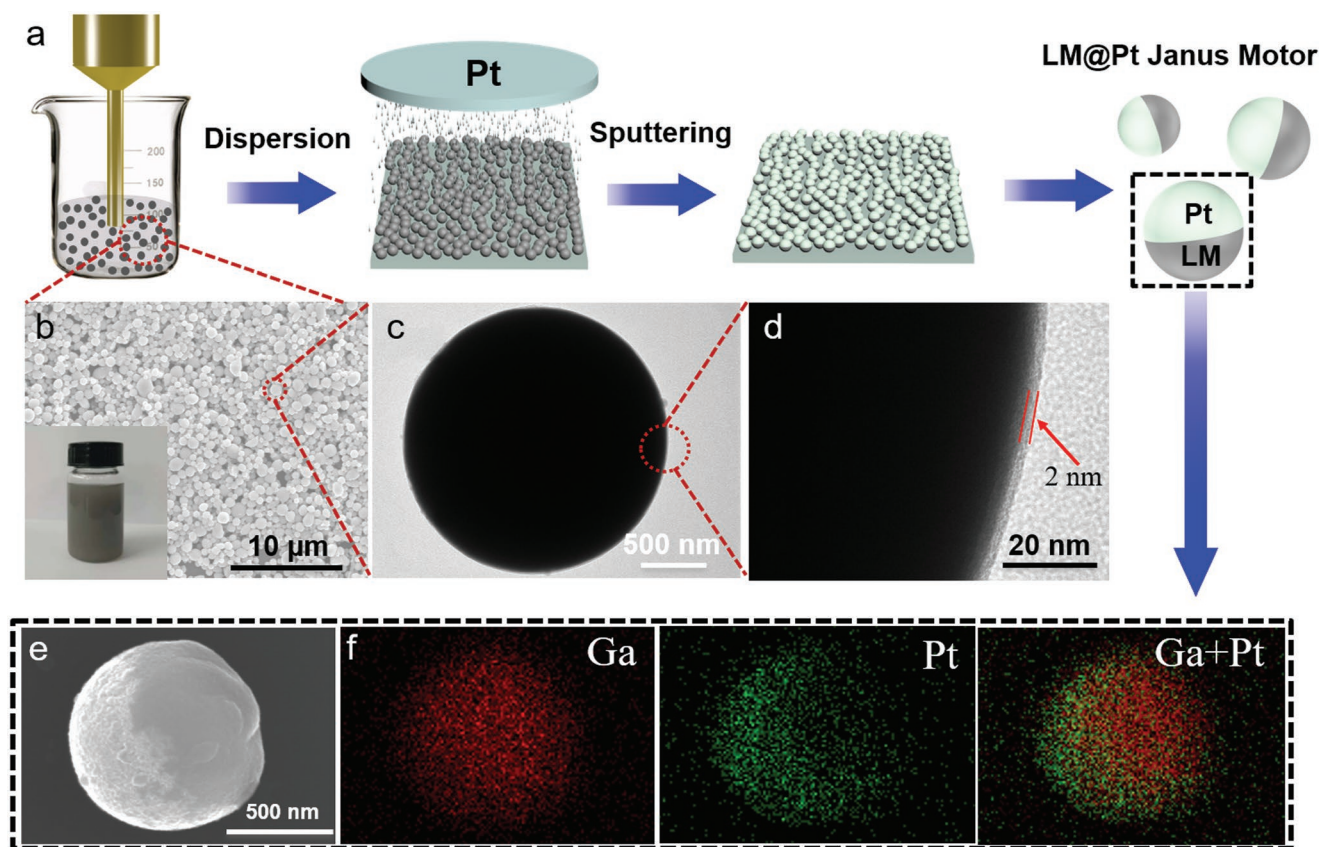


**Figure 1.** Fabrication and characterization of LM–Pt Janus particles. a) Fabrication of the LM–Pt Janus particles via sputtering Pt onto LM monolayers. b) SEM image of the LM spheres fabricated by ultrasonic dispersion. Inset: the obtained LM spheres are uniformly dispersed in ethanol. c) TEM image of an LM sphere. d) A thin  $\text{Ga}_2\text{O}_3$  shell on the LM sphere. e) SEM image of a fabricated LM–Pt Janus sphere. f) EDS elemental mapping of the LM–Pt Janus sphere from (e) showing a Janus structure.

Herein, we report a new type of LM–MNM with dimensions ranging from hundreds of nanometers to a few micrometers, capable of moving through self-electrophoresis by electrochemically converting  $\text{H}_2\text{O}_2$ . The Janus structure of LM–MNMs is fabricated by sputtering Pt onto one hemisphere of an LM microsphere produced by ultrasonic dispersion. They can reach peak velocities of  $\approx 30 \mu\text{m s}^{-1}$  without any visible bubbles emerging from their tails. To showcase their potential usefulness, we provide a proof-of-concept where these chemically powered LM–MNMs are employed as intelligent microfillers that target and weld silver nanowires (AgNWs), thereby greatly improving the electrical conductivity of the AgNW network. This represents, to the best of our knowledge, the first report of chemically powered LM–MNMs operating at micro- and nanoscales, and also the first application of MNMs of any kind to carry out micro-welding. By combining the unique properties of liquid metals with the propulsion and targeting capabilities of MNMs, this work provides a glimpse of the wide range of potential applications of LM–MNMs that extend far beyond the precise circuit repair and microwelding demonstrated here to fields like nanomedicine and bioimaging.

For the fabrication of our LM–MNM Janus motors (Figure 1), we used Galinstan with a composition of 68.5% gallium, 21.5% indium, and 10% tin and a melting point well below room temperature.<sup>[19]</sup> Furthermore, we used an ultrasound

sonifier to disperse the LM bulk material in ethanol into micro/nanoparticles, which were then arranged into a monolayer on a glass substrate (see the Experimental Section). Then, a thin layer (about  $\approx 10 \text{ nm}$ ) of metal (e.g., Pt, Ag, or Au) was deposited onto the top hemisphere of the particles using a sputter machine to produce the Janus particles. The resulting LM micro/nanoparticles are roughly spherical (Figure 1b) with user-controllable size distribution (tunable by adjusting the ultrasonic treatment parameters—Figure S1, Supporting Information). The Janus structure of the fabricated LM–MNM was confirmed through scanning electron microscopy (SEM) and elemental mapping by energy dispersive spectroscopy (EDS) (Figure 1e,f). Notably, smaller LM particles can be obtained by increasing the power and duration of the ultrasound dispersion (see below).

One notable feature of the dispersed LM particles is a thin surface layer of  $\text{Ga}_2\text{O}_3$ , which is known to spontaneously and rapidly form as Galinstan is exposed to the oxygen in air (or water in our case).<sup>[20]</sup> Through high resolution transmission electron microscopy (TEM), we determined the layer thickness as  $\approx 2 \text{ nm}$  (Figure 1c,d). This ultrathin oxide layer is important for three reasons. First, its presence maintains the spherical shape of the LM particles and prevents them from merging uncontrollably. Second, being a semiconductor, a  $\text{Ga}_2\text{O}_3$  layer allows for electron transfer between the Pt layer

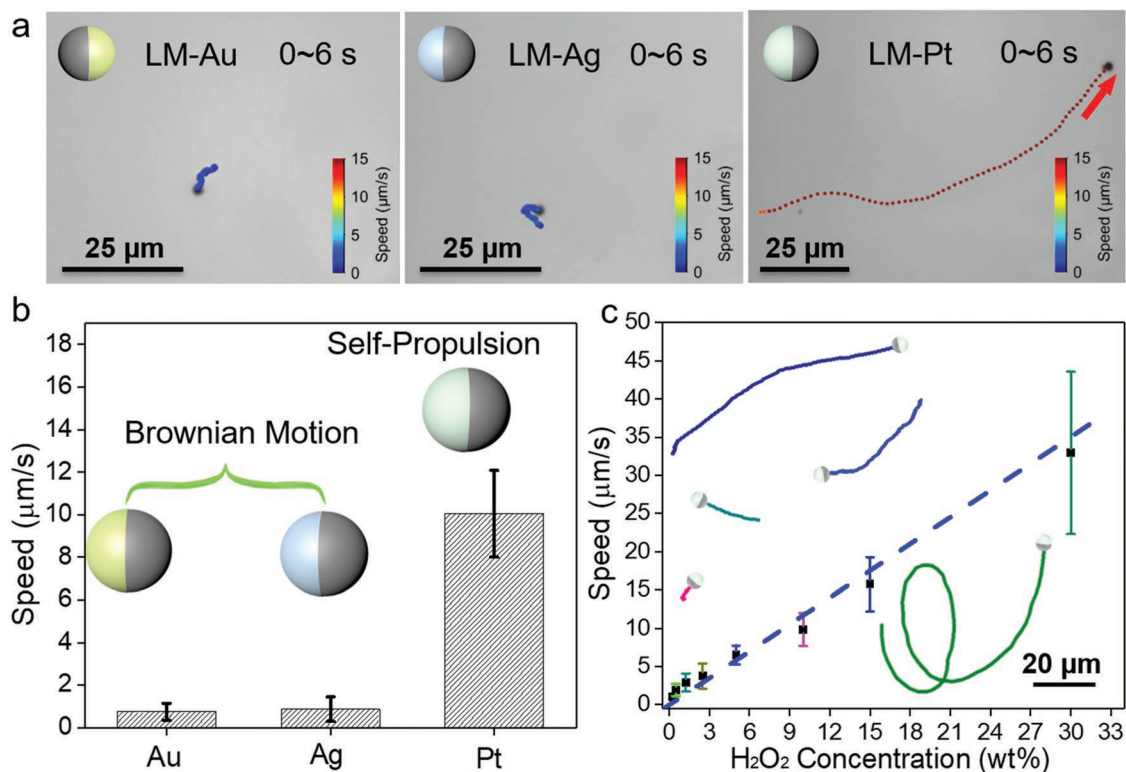


**Figure 2.** LM-MNM speeds for different metal coatings and  $\text{H}_2\text{O}_2$  concentrations. a) Video snapshots of LM-MNMs with Au, Ag, and Pt coatings in 10 wt%  $\text{H}_2\text{O}_2$  recorded for a period of 6 s. b) Average speed of LM-MNMs half coated with Au, Ag, and Pt. c) Average speed of Pt-coated LM-MNMs swimming in different concentrations of  $\text{H}_2\text{O}_2$  (squares) and corresponding trajectories during 6 s (trajectories are matched to data points by colors). Error bars indicate standard deviation ( $N = 10$ ).

and the LM core via electron tunneling,<sup>[21]</sup> which is necessary for self-electrophoresis to occur (see below). Third, this layer readily dissolves in diluted hydrochloric acid ( $\text{pH} = 0.4$ ), thus enabling us to exploit the fluidic nature of the LM particles in a microwelding application demonstrated at the end of this article.

Upon being added to an aqueous solution containing  $\text{H}_2\text{O}_2$ , Pt-coated LM micro/nanoparticles transform into micro- and nanomotors and begin to move around rapidly. Typical trajectories of moving LM-MNMs are shown in Movie S1 in the Supporting Information and Figure 2a,c. This result is further investigated by varying three key experimental parameters: the type of metal coating, the  $\text{H}_2\text{O}_2$  concentration, and the particle size.

**Metal Coating:** While LM-MNMs coated with Au or Ag layer only exhibited a Brownian-like motion with very low activity even in the presence of 10 wt%  $\text{H}_2\text{O}_2$  (Figure 2a,b), Pt-coated LM-MNMs achieved much higher velocities. It seems that the presence of highly catalytic Pt is crucial for the self-propulsion of the LM-MNMs, and that the catalytic reaction of  $\text{H}_2\text{O}_2$  decomposition provides the necessary energy. While this may appear similar to typical Pt-coated  $\text{SiO}_2$ <sup>[22]</sup> micromotors, we will show below that our MNMs operate by a different mechanism. We would also like to emphasize that we did not observe any bubbles in the immediate vicinity of a moving LM-MNMs, even at very high fuel concentrations (30%  $\text{H}_2\text{O}_2$ ) thus ruling out bubble propulsion.<sup>[23]</sup>

**$\text{H}_2\text{O}_2$  Concentration:** It is known that the activity of chemically propelled MNMs largely depends on fuel concentrations. By increasing the  $\text{H}_2\text{O}_2$  concentrations from 0.25 to 30 wt%, the LM-MNM velocities increased almost linearly from  $1.0 \pm 0.5$  to  $32.9 \pm 11 \mu\text{m s}^{-1}$  (Figure 2c, linear fit  $R_2 = 0.91$ ). This continued increase is somewhat surprising since the speeds of chemical MNMs typically reach a plateau at high fuel concentrations once the speed becomes limited by the surface reaction kinetics rather than the diffusion of fuel molecules.<sup>[24]</sup> The fact that we did not reach any plateau suggests that the reaction kinetics, of whatever the reaction might be, are very fast indeed.

**Particle Size:** The last experimental parameter we investigated is the LM-MNM size. As mentioned earlier, the LM particle size can be controlled by tuning the power and duration of the ultrasonic dispersion process. Here, we focus on two batches of LM particles: one batch with diameters of 500–800 nm ( $650 \pm 150$  nm) and a second batch with particle sizes ranging from 2–10  $\mu\text{m}$ .

Considering the strong Brownian motion of nanosized motors, the self-propulsion behavior of the 500–800 nm particles is characterized by an enhanced diffusion coefficient rather than an instantaneous speed<sup>[25]</sup> (Movie S2, Supporting Information). The mean squared displacement (MSD) of some typical LM nanomotors (LM-NMs) in different  $\text{H}_2\text{O}_2$  concentrations is shown in Figure 3a. Their diffusion coefficients,  $D$ , can be extracted from the slope of the linear segments of the MSD plots according to  $\text{MSD} = 4D\Delta t$  (only diffusion in



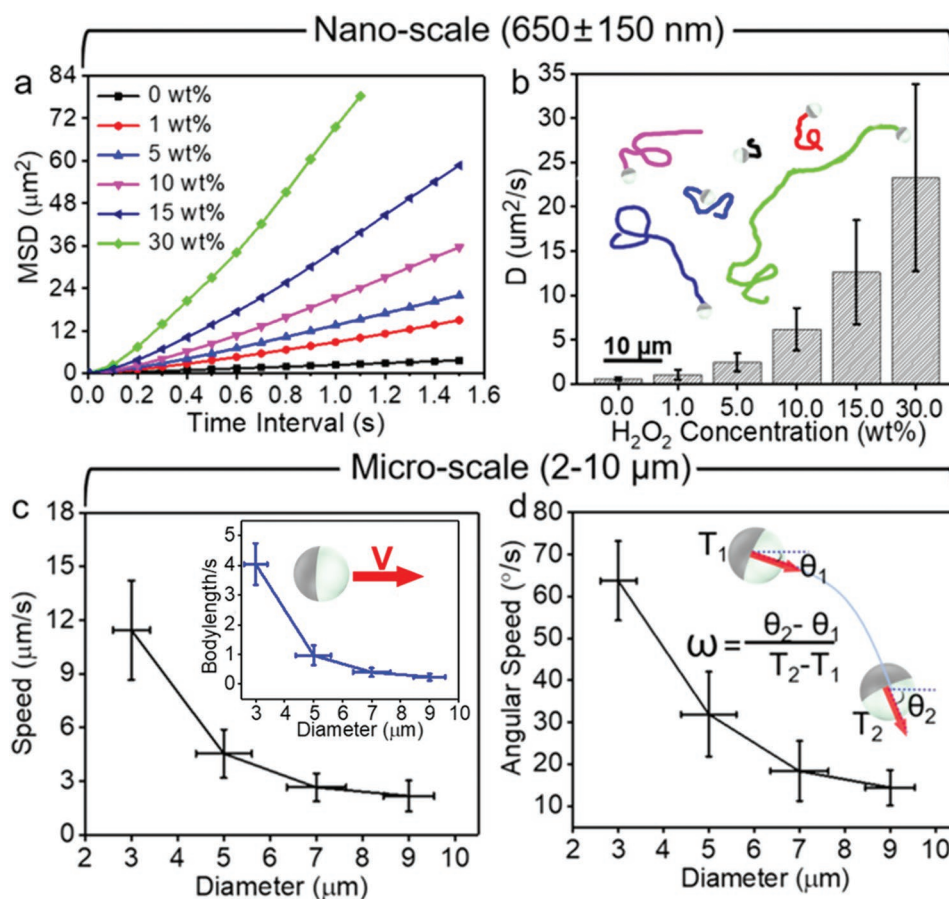


**Figure 3.** Size-dependent dynamics of LM-MNMs. a) MSD as a function of time interval in different  $\text{H}_2\text{O}_2$  concentrations. b) Diffusion coefficients (bars) and typical trajectories (lines—the colors correspond to those from (a)) for different  $\text{H}_2\text{O}_2$  concentrations. c) LM-MM speed as a function of particle diameter in 10 wt%  $\text{H}_2\text{O}_2$ . Inset: speeds in units of body-lengths per second. d) Angular velocities of differently sized LM-MMs and a schematic illustrating the calculation of angular velocities. Error bars indicate standard deviation ( $N = 10$ ).

2D is considered).<sup>[26]</sup>  $D$  increased from  $0.64 \pm 0.17 \mu\text{m}^2 \text{s}^{-1}$  for 0 wt%  $\text{H}_2\text{O}_2$  (commensurate with the theoretical value of purely Brownian motion), to  $23.36 \pm 10.47 \mu\text{m}^2 \text{s}^{-1}$  at 30 wt%  $\text{H}_2\text{O}_2$  (Figure 3b). Typical particle tracks are shown to help visualize the difference in activity (Figure 3b). In addition, due to highly efficient self-propulsion and its sustained duration, the active motion of LM-NMs changed from enhanced diffusion to long-range ballistic self-propulsion.

In contrast, the microsized LM motors (2–10  $\mu\text{m}$ ) exhibited insignificant Brownian motion. Furthermore, the speeds of the LM-MMs decreased with increasing particle diameters (Figure 3c). A typical video of the size dependent self-propulsion of the LM-MMs is provided in Movie S3 in the Supporting Information. This result agrees with previous studies on chemically propelled MNM systems.<sup>[27]</sup> Not only do larger motors move more slowly, they also move with an improved directionality. This can be shown by calculating the average angular speed of moving LM-MMs as a function of motor size (Figure 3d). The angular speed decreased quickly from about  $63 \pm 10^\circ \text{s}^{-1}$  for LM-MMs of diameters  $3 \pm 0.4 \mu\text{m}$  to  $15 \pm 3^\circ \text{s}^{-1}$  for particle diameters of  $9 \pm 0.6 \mu\text{m}$ , indicating that larger LM-MMs move along more straight trajectories.

After investigating the effects of different particle and environmental parameters on LM-MNM dynamics, we now turn our focus to the propulsion mechanism itself. Most typical propulsion mechanisms for chemically driven micromotors can be easily ruled out: bubble propulsion is unlikely as we did not observe any bubbles in the experiments; also the Marangoni effect which propels particles via surface tension gradients can be ruled out as this effect does not usually occur with micro/nanoscale particles or with particles moving in aqueous solution rather than on a liquid–air interface.<sup>[28]</sup> Another popular mechanism is self-diffusiophoresis through surface chemical reactions that result in a local gradient of chemicals.<sup>[29]</sup> Unlike the Pt-coated  $\text{SiO}_2$  or PS spheres,<sup>[30]</sup> the LM-MNMs in our experiments moved significantly faster than Pt-coated  $\text{SiO}_2$  motors fabricated in the same way. We believe that the most plausible explanation that aligns with our experimental observations is that our LM-MNMs are driven by an asymmetric distribution of protons which creates an electric field that propels the motors via self-electrophoresis, much in the same way as a bimetallic micromotor<sup>[31,32]</sup> (see Figure 4a). To explain this propulsion mechanism, let us assume that the  $\text{H}_2\text{O}_2$  on the surface of the LM-MNMs Pt coating electrochemically decomposes in a similar fashion to an Au–Pt microsphere.<sup>[33]</sup> The Pt hemisphere

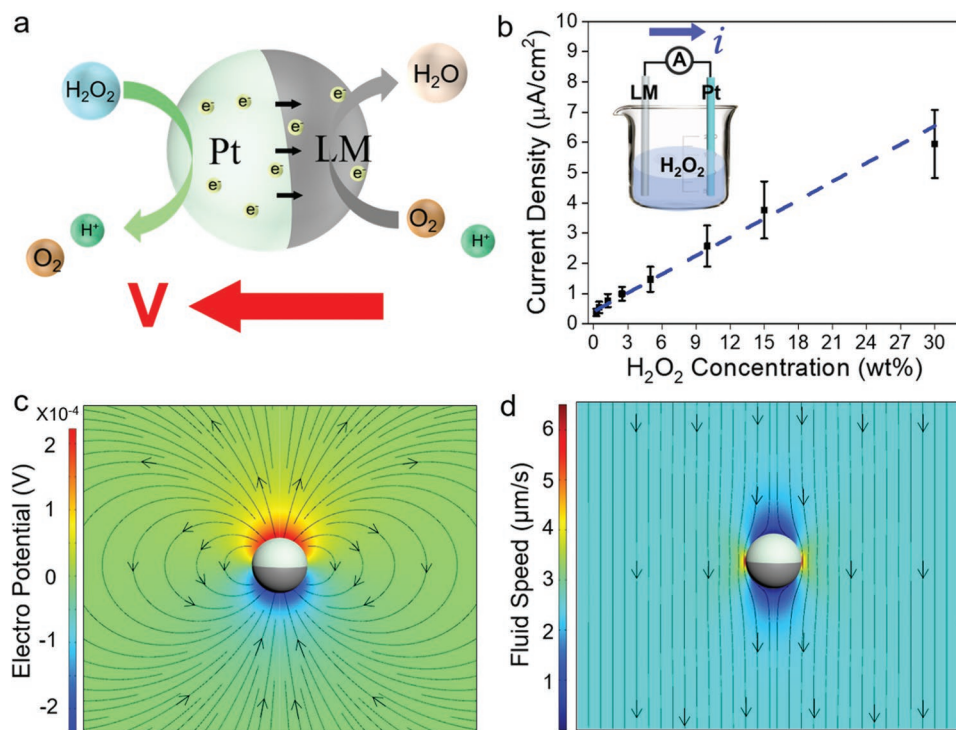


**Figure 4.** Self-electrophoresis mechanism of LM-MNMs in H<sub>2</sub>O<sub>2</sub>. a) Schematic illustrating the self-propulsion mechanism due to oxidation on the Pt side and reduction at the uncoated hemisphere. b) Electrochemical measurement of the current density of the LM–Pt system (error bars indicate standard deviation,  $N = 10$ ) for different H<sub>2</sub>O<sub>2</sub> concentrations; the inset illustrates the experimental setup. c,d) Simulated results of the electrical potential (c) and the fluid field around a self-propelled LM–MNM (d).

preferentially catalyzes the oxidation of H<sub>2</sub>O<sub>2</sub> and generates an excess of protons as the electrons migrate via the conductive core from the Pt side to the uncoated side where they reduce H<sub>2</sub>O<sub>2</sub> (or O<sub>2</sub>) into water. This resulting asymmetric distribution of protons creates an electric field that propels the motors via self-electrophoresis.

Since a motor undergoing self-electrophoresis is essentially a battery in short circuit, an electric current must flow from the cathode to the anode. To test this hypothesis, we carried out electrochemical measurements (similar to previous studies<sup>[32,34]</sup>) to confirm the existence of the current flow and thus to confirm that self-electrophoresis is indeed the driving mechanism of our LM-MNMs. We measured the electrical current between the Pt electrode and LM electrode immersed in H<sub>2</sub>O<sub>2</sub> solution (Figure 4b inset for setup; see the Supporting Information for experimental details), which confirms our hypothesis. More importantly, the current density increased linearly ( $R_2 = 0.98$ ) from  $0.38 \pm 0.10$  to  $5.9 \pm 1.1 \mu\text{A cm}^{-2}$  when increasing the H<sub>2</sub>O<sub>2</sub> concentration from 0.25 to 30 wt% (Figure 4b, Figure S2a, Supporting Information), suggesting that the current density of the electrochemical reaction is directly correlated with the self-propulsion velocity (Figure S2b, Supporting Information). Moreover, the current density of LM–Au and LM–Ag (Figure S2c, Supporting Information) combinations are much lower than that of LM–Pt, which is in good agreement with our observations that LM–Au and LM–Ag Janus particles hardly moved (Figure 2a). All these electrochemical measurements lend strong support to our hypothesis of a self-electrophoresis mechanism.

To obtain more conclusive evidence and in an effort to quantitatively reproduce the observed motor speeds, we performed numerical simulations using an electrokinetic model reported previously<sup>[35,36]</sup> (see Figures S3 and S4 in the Supporting Information). Our model is based on two important assumptions: i) the electrical double-layer on the motor surface is assumed to be thin and not significantly perturbed by the surface reactions, and ii) the chemical reaction rate on the motor surface is assumed to be constant and uniform while proton fluxes normal to the surface are assumed to be equal and opposite on the anode and cathode sides of the motor. The flux is measured using the current density as a proxy (Figure 4b). The simulated distributions of the electric potential (Figure 4c) and flow field (Figure 4d) show a typical self-electrophoretic micromotor moving away from the cathode end. From the flux numbers extracted from electrochemical measurements (Figure 3b), we obtained motor speeds of  $1.74 \mu\text{m s}^{-1}$ . This suggests that our proposed self-electrophoresis mechanism can provide a sufficiently strong propulsive force to move an LM-MNM with speeds comparable to those observed in our experiments. We note, however, that our simulation could not explain the particle size dependence of the motor speeds, which could be due to the charged bottom substrate that is known to slow down electrophoretic micromotors<sup>[35,37]</sup> but was not considered in our model.

So far, we mostly considered the moving liquid metal microsphere as a solid particle and discussed its single-particle dynamics and propulsion mechanisms. Next, we would like to highlight a potential example application of

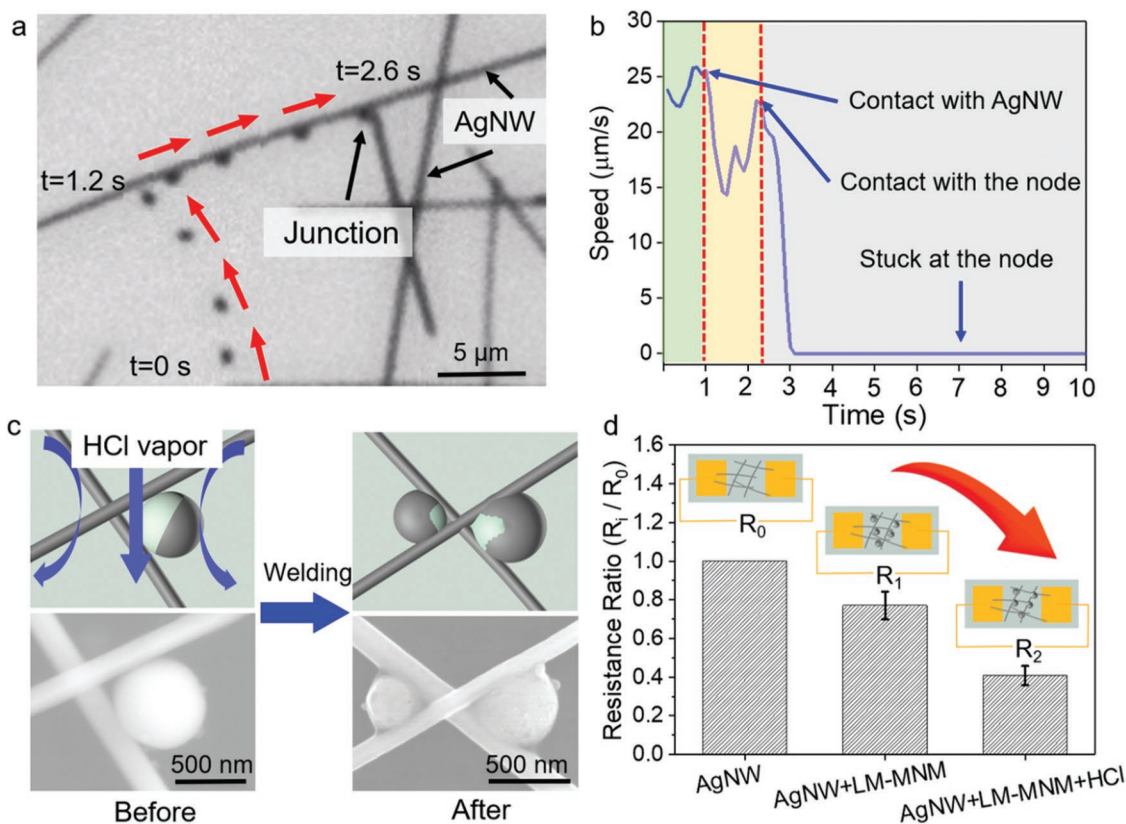


**Figure 5.** Microwelding of AgNW by self-propelled LM-MNMs. a) Video snapshot and b) instantaneous speed of a LM-MNM moving within the AgNW network. c) Schematic illustrating the HCl vapor treatment and the corresponding SEM images of LM-MNMs stuck at an AgNW junction before and after microwelding. d) Electrical resistance of a gapped gold electrode under different conditions: with AgNW network only ( $R_0$ ), and with AgNW and LM-MNMs before ( $R_1$ ) and after ( $R_2$ ) microwelding, respectively. (Error bars indicate standard deviation,  $N = 6$ ).

LM-MNMs that arises from their unique material properties: microwelding. We choose a AgNW network as our model scenario considering their wide use in electronic devices.<sup>[38]</sup> Particularly, the contact resistance at AgNW junctions has been a long-standing challenge for AgNW-based transparent conductive film applications.<sup>[39]</sup> Below, we demonstrate how LM-MNMs can serve as intelligent robotics devices that autonomously find and weld the cross-junctions of a AgNW network, and in doing so greatly reduce its contact resistance.

LM-MNMs tend to move along the AgNWs upon contacting the nanowires, with the AgNWs serving as guide tracks for the self-propelled motors (Figure 5a; Movie S4, Supporting Information). Structures providing guidance to motors has been reported previously.<sup>[40]</sup> Importantly, when the LM-MNMs encounter the junctions of the AgNW network, they can get stuck, thereby facilitating the subsequent welding process (see below).

Although flexible and conductive, the LM-MNMs stuck at the junctions are not yet capable of significantly reducing the contact resistance because: i) they are still in point contact with the nearby AgNWs and cannot form a robust bond, and ii) there is a thin oxide layer of  $\text{Ga}_2\text{O}_3$  on the LM-MNM surface. In order to further reduce the contact resistance, we exposed the entire thin film with LM-MNM trapped at AgNWs junctions to acid vapor (Figure S5 and Movie S5, Supporting Information), which resulted in the rapid removal of the  $\text{Ga}_2\text{O}_3$  layer

(Figure 5c; Figure S6, Supporting Information). The acid treatment exposed pristine LM surfaces that readily formed metallic bonds with silver at the junctions of the AgNWs. LM-MNMs essentially served as fillers welding the AgNWs together. To examine the effect of this microwelding on reducing the contact resistance, we measured the electrical resistance of an Au electrode (Figure S7, Supporting Information) on a glass slide where an AgNW network bridged the electrode gap. The resistances of the electrode after different treatment were normalized according to the initial resistance value ( $R_0$ ) of electrodes with AgNW network only. After adding LM-MNMs, the resistance ( $R_1$ ) reduced to be 77% of  $R_0$  because of the presence of LM-MNMs particles at the junctions of the AgNW networks. Then, the resistance after welding ( $R_2$ ) by acid treatment further decreased to be only about 40%, suggesting that LM-MNMs indeed welded the AgNW junctions and lowered the contact resistance (Figure 5d).

In summary, we have presented a liquid-metal-based deformable micro/nanomotor that is chemically self-propelled by self-electrophoresis. The spherical LM-MNMs were of a classical Janus structure, i.e., half-coated with Pt that catalyzes the decomposition of  $\text{H}_2\text{O}_2$  fuel to harness energy for self-propulsion. Through electrochemical measurements and numerical simulations, we tentatively identify the self-propulsion mechanism of the LM-MNMs as self-electrophoresis. Furthermore, we systematically investigated the dependence of LM-MNM



dynamics on fuel concentrations, coating metal types, and motor sizes. Due to their active self-propulsion, LM-MNMs can approach and move along AgNW networks until they become stuck at a junction. Such a spontaneous process enables the LM-MNMs to actively “search” for the target sites within the AgNW network, where they then perform microwelding to bond the AgNW junctions and lower the contact resistance as a result of their liquid metal nature. This work provided a preliminary but novel application of LM-MNMs for circuit repair or circuit bonding at small scales. Despite being rather primitive and limited, our chemically powered LM-MNMs could provide the necessary inspiration to create novel applications in a number of disciplines including robotics, material sciences, and biomedical engineering.

## Experimental Section

**Materials and Instruments:** Liquid metal (Galinstan consisting of 68.5% gallium, 21.5% indium, and 10% tin), ethanol (>99%), hydrogen peroxide (H<sub>2</sub>O<sub>2</sub>, 30 wt%), and hydrogen chloride (HCl, 37%) were commercially purchased and used as received. An ultrasonic homogenizer (NingBo Scientz Biotechnology JY92-II DN) was used to break the LM into micro/nanoparticles. Their sizes and zeta potential were measured with a Zetasizer Nano ZSP (Malvern). A sputter machine (Kyky Technology; SBC-12) was used to coat a layer of platinum on the surface of the LM particles. A field-emission scanning electron microscope (FESEM; Hitachi S4700) and transmission electron microscope (Tecnai G2 Spirit) were used for SEM and TEM imaging. Videos showing the motors' movements were captured via inverted optical microscopy using a digital camera (Lecia DMI8) at about 10 fps. Motor dynamics were tracked and analyzed by ImageJ.<sup>[41]</sup>

**Synthesis of LM-MNMs:** First, LM (20 μL) was added to 15 mL of ethanol and the container was kept in an ice bath. Then, probe sonication (300 W) was applied to break up the LM into small particles with the power and treatment time (up to 30 min) chosen accordingly in order to obtain different size distributions of the LM micro/nanoparticles (LM-MNPs). The synthesized LM-MNPs (ethanol suspension) were dropped uniformly onto a precleaned glass slide by O<sub>2</sub> plasma treatment for 3 min to form a monolayer. A proper concentration of the LM-MNPs suspension (about 2 mg mL<sup>-1</sup>) was chosen in order to ensure monolayer formation instead of forming multiple layers. Then, the monolayer of LM-MNPs was half-coated with a thin layer of different metallic materials (Pt, Au, or Ag) using a sputter machine. Finally, the formed LM-MNMs were collected from the glass slide by bath sonication at low power (80 W) for about 30 s in order to avoid affecting the particles size and shape. Then, the LM-MNMs were dispersed in deionized water for further use.

**Electrochemical Measurements:** An electrochemical workstation (Shanghai Chenhua Instrument; CHI760E) was used to measure the *i*-*t* curve and open circuit potential (OCP). The working electrode was connected to the LM and the reference and counter electrodes were both connected to the metal (Pt, Au, or Ag) electrode. The different materials (Pt, Au, and Ag) were sputtered onto an aluminum foil to form the Pt, Au, and Ag electrodes. Then, the working electrode was connected to a copper wire that was inserted into a large LM droplet serving as the LM electrode. Different concentrations of H<sub>2</sub>O<sub>2</sub> were added to the beaker and the *i*-*t* curve or open circuit voltage was measured for 60 s.

**HCl Vapor Treatment, Vessel Design, and Fabrication:** Solidworks was used for the design of the treatment vessel which was fabricated by 3D printing (SPSS-450). The vessel contained four sites for the sample loading and a sieve plate was placed above the samples to ensure uniform treatment by HCl vapor as shown in Movie S6 in the Supporting Information. Then, HCl vapor was pumped into the vessel along with compressed nitrogen from the inlets to react with the sample (Ag NWs+LM-MNMs).

## Supporting Information

Supporting Information is available from the Wiley Online Library or from the author.

## Acknowledgements

The authors thank the financial support from the National Natural Science Foundation of China (51802060 and 11774075), the Shenzhen Innovation Project (KQJSCX20170726104623185), the Shenzhen Peacock Group (KQTD20170809110344233), and the Natural Science Foundation of Guangdong Province (No. 2017B030306005).

## Conflict of Interest

The authors declare no conflict of interest.

## Keywords

liquid metals, micro/nanomotors, microwelding, self-electrophoresis

Received: August 6, 2019

Revised: October 3, 2019

Published online:

- [1] F. Wong, K. K. Dey, A. Sen, *Annu. Rev. Mater. Res.* **2016**, *46*, 407.
- [2] a) T. E. Mallouk, A. Sen, *Sci. Am.* **2009**, *300*, 72; b) X. Chen, C. Zhou, W. Wang, *Chem.-Asian J.* **2019**, *14*, 2388.
- [3] a) S. Fournier-Bidoz, A. C. Arsenault, I. Manners, G. A. Ozin, *Chem. Commun.* **2005**, 441; b) W. F. Paxton, K. C. Kistler, C. C. Olmeda, A. Sen, S. K. St. Angelo, Y. Y. Cao, T. E. Mallouk, P. E. Lammert, V. H. Crespi, *J. Am. Chem. Soc.* **2004**, *126*, 13424.
- [4] a) L. Baraban, D. Makarov, R. Streubel, I. Moench, D. Grimm, S. Sanchez, O. G. Schmidt, *ACS Nano* **2012**, *6*, 3383; b) A. Q. Ansari, S. J. Ansari, M. Q. Khan, M. F. Khan, U. A. Qureshi, Z. Khatir, F. Ahmed, I. S. Kim, *Mater. Res. Express* **2019**, *6*, 075405; c) V. Garcia-Gradilla, J. Orozco, S. Sattayasamitsathit, F. Soto, F. Kuralay, A. Pourazary, A. Katzenberg, W. Gao, Y. Shen, J. Wang, *ACS Nano* **2013**, *7*, 9232.
- [5] Z. Wu, J. Troll, H.-H. Jeong, Q. Wei, M. Stang, F. Ziemssen, Z. Wang, M. Dong, S. Schnichels, T. Qiu, P. Fischer, *Sci. Adv.* **2018**, *4*, eaat4388.
- [6] a) Y. Wang, C. Zhou, W. Wang, D. Xu, F. Zeng, C. Zhan, J. Gu, M. Li, W. Zhao, J. Zhang, J. Guo, H. Feng, X. Ma, *Angew. Chem., Int. Ed.* **2018**, *57*, 13110; b) M. Liu, Y. Sun, T. Wang, Z. Ye, H. Zhang, B. Dong, C. Y. Li, *J. Mater. Chem. C* **2016**, *4*, 5945; c) M. Guix, C. C. Mayorga-Martinez, A. Merkoci, *Chem. Rev.* **2014**, *114*, 6285.
- [7] a) D. Vilela, M. M. Stanton, J. Parmar, S. Sanchez, *ACS Appl. Mater. Interfaces* **2017**, *9*, 22093; b) D. Vilela, J. Parmar, Y. Zeng, Y. Zhao, S. Sanchez, *Nano Lett.* **2016**, *16*, 2860; c) M. Safdar, S. U. Khan, J. Janis, *Adv. Mater.* **2018**, *30*, 1703660; d) H. Ceylan, J. Giltinan, K. Kozielski, M. Sitti, *Lab Chip* **2017**, *17*, 1705; e) M. Safdar, J. Simmchen, J. Janis, *Environ. Sci.: Nano* **2017**, *4*, 2235; f) C. Liang, C. Zhan, F. Zeng, D. Xu, Y. Wang, W. Zhao, J. Zhang, J. Guo, H. Feng, X. Ma, *ACS Appl. Mater. Interfaces* **2018**, *10*, 35099.
- [8] a) J. M. Yeomans, *Nat. Mater.* **2014**, *13*, 1004; b) T. Sanchez, D. T. N. Chen, S. J. DeCamp, M. Heymann, Z. Dogic, *Nature* **2012**, *491*, 431; c) M. C. Marchetti, J. F. Joanny, S. Ramaswamy, T. B. Liverpool, J. Prost, M. Rao, R. A. Simha, *Rev. Mod. Phys.* **2013**, *85*, 1143.

- [9] H. Wang, M. Pumera, *Chem. Rev.* **2015**, *115*, 8704.
- [10] a) S. Sánchez, L. Soler, J. Katuri, *Angew. Chem., Int. Ed.* **2015**, *54*, 1414; b) S. Wang, X. Liu, Y. Wang, D. Xu, C. Liang, J. Guo, X. Ma, *Nanoscale* **2019**, *11*, 14099.
- [11] S.-Y. Tang, D. R. Mitchell, Q. Zhao, D. Yuan, G. Yun, Y. Zhang, R. Qiao, Y. Lin, M. D. Dickey, W. Li, *Matter* **2019**, *1*, 192.
- [12] a) J. C. Yeo, J. Yu, Z. M. Koh, Z. Wang, C. T. Lim, *Lab Chip* **2016**, *16*, 3244; b) J. W. Boley, E. L. White, G. T. C. Chiu, R. K. Kramer, *Adv. Funct. Mater.* **2014**, *24*, 3501; c) Q. Wang, Y. Yu, J. Yang, J. Liu, *Adv. Mater.* **2015**, *27*, 7109; d) J. Yoon, S. Y. Hong, Y. Lim, S.-J. Lee, G. Zi, J. S. Ha, *Adv. Mater.* **2014**, *26*, 6580; e) Q. Wang, R. Guo, M. Zhang, S. Wang, C. Lu, M. Xue, J.-B. Fan, Z.-Z. He, W. Rao, *Mater. Horiz.* **2019**, *6*, 1643.
- [13] a) Q. Wang, Y. Yu, K. Pan, J. Liu, *IEEE Trans. Biomed. Eng.* **2014**, *61*, 2161; b) S. A. Chechetka, Y. Yu, X. Zhen, M. Pramanik, K. Pu, E. Miyako, *Nat. Commun.* **2017**, *8*, 15432.
- [14] a) S. Handschuh-Wang, Y. Chen, L. Zhu, T. Gan, X. Zhou, *Langmuir* **2019**, *35*, 372; b) S. Y. Tang, V. Sivan, P. Petersen, W. Zhang, P. D. Morrison, K. Kalantar-zadeh, A. Mitchell, K. Khoshmanesh, *Adv. Funct. Mater.* **2014**, *24*, 5851; c) S.-C. Tan, B. Yuan, J. Liu, *Proc. R. Soc. A* **2015**, *471*, 20150297.
- [15] A. Zavabeti, T. Daeneke, A. F. Chrimes, A. P. O'Mullane, J. Z. Ou, A. Mitchell, K. Khoshmanesh, K. Kalantar-zadeh, *Nat. Commun.* **2016**, *7*, 12402.
- [16] a) J. Zhang, Y. Yao, L. Sheng, J. Liu, *Adv. Mater.* **2015**, *27*, 2648; b) B. Yuan, S. Tan, Y. Zhou, J. Liu, *Sci. Bull.* **2015**, *60*, 1203.
- [17] X. Tang, S.-Y. Tang, V. Sivan, W. Zhang, A. Mitchell, K. Kalantar-zadeh, K. Khoshmanesh, *Appl. Phys. Lett.* **2013**, *103*, 174104.
- [18] D. Wang, C. Gao, W. Wang, M. Sun, B. Guo, H. Xie, Q. He, *ACS Nano* **2018**, *12*, 10212.
- [19] T. Liu, P. Sen, C.-J. Kim, *J. Microelectromech. Syst.* **2011**, *21*, 443.
- [20] W. Zhang, J. Z. Ou, S.-Y. Tang, V. Sivan, D. D. Yao, K. Latham, K. Khoshmanesh, A. Mitchell, A. P. O'Mullane, K. Kalantar-zadeh, *Adv. Funct. Mater.* **2014**, *24*, 3799.
- [21] J. Ma, M. Zheng, C. Chen, Z. Zhu, X. Zheng, Z. Chen, Y. Guo, C. Liu, Y. Yan, G. Fang, *Adv. Funct. Mater.* **2018**, *28*, 1804128.
- [22] J. G. Gibbs, Y.-P. Zhao, *Appl. Phys. Lett.* **2009**, *94*, 163104.
- [23] J. Orozco, B. Jurado-Sanchez, G. Wagner, W. Gao, R. Vazquez-Duhalt, S. Sattayasamitsathit, M. Galarnyk, A. Cortes, D. Saintillan, J. Wang, *Langmuir* **2014**, *30*, 5082.
- [24] W. F. Paxton, A. Sen, T. E. Mallouk, *Chem. - Eur. J.* **2005**, *11*, 6462.
- [25] T.-C. Lee, M. Alarcon-Correa, C. Miksch, K. Hahn, J. G. Gibbs, P. Fischer, *Nano Lett.* **2014**, *14*, 2407.
- [26] P. Schattling, B. Thingholm, B. Stadler, *Chem. Mater.* **2015**, *27*, 7412.
- [27] a) S. Ebbens, M.-H. Tu, J. R. Howse, R. Golestanian, *Phys. Rev. E* **2012**, *85*, 020401; b) H. Wang, J. G. S. Moo, M. Pumera, *ACS Nano* **2016**, *10*, 5041.
- [28] Y.-J. Chen, Y. Nagamine, K. Yoshikawa, *Phys. Rev. E* **2009**, *80*, 016303.
- [29] a) A. Würger, *Phys. Rev. Lett.* **2015**, *115*, 188304; b) F. Yang, S. Qian, Y. Zhao, R. Qiao, *Langmuir* **2016**, *32*, 5580; c) M. N. Popescu, W. E. Uspal, S. Dietrich, *Eur. Phys. J.: Spec. Top.* **2016**, *225*, 2189.
- [30] a) A. T. Brown, W. C. K. Poon, C. Holm, J. de Graaf, *Soft Matter* **2017**, *13*, 1200; b) A. Brown, W. Poon, *Soft Matter* **2014**, *10*, 4016; c) S. Ebbens, D. A. Gregory, G. Dunderdale, J. R. Howse, Y. Ibrahim, T. B. Liverpool, R. Golestanian, *EPL* **2014**, *106*, 58003.
- [31] W. F. Paxton, P. T. Baker, T. R. Kline, Y. Wang, T. E. Mallouk, A. Sen, *J. Am. Chem. Soc.* **2006**, *128*, 14881.
- [32] Y. Wang, R. M. Hernandez, D. J. Bartlett Jr., J. M. Bingham, T. R. Kline, A. Sen, T. E. Mallouk, *Langmuir* **2006**, *22*, 10451.
- [33] P. M. Wheat, N. A. Marine, J. L. Moran, J. D. Posner, *Langmuir* **2010**, *26*, 13052.
- [34] R. Liu, A. Sen, *Abstr. Pap. Am. Chem. Soc.* **2012**, *243*, 20064.
- [35] W. Wang, T.-Y. Chiang, D. Velegol, T. E. Mallouk, *J. Am. Chem. Soc.* **2013**, *135*, 10557.
- [36] W. Wang, W. Duan, A. Sen, T. E. Mallouk, *Proc. Natl. Acad. Sci. USA* **2013**, *110*, 17744.
- [37] a) T.-Y. Chiang, D. Velegol, *Langmuir* **2014**, *30*, 2600; b) M. Wei, C. Zhou, J. Tang, W. Wang, *ACS Appl. Mater. Interfaces* **2018**, *10*, 2249.
- [38] a) S. De, T. M. Higgins, P. E. Lyons, E. M. Doherty, P. N. Nirmalraj, W. J. Blau, J. J. Boland, J. N. Coleman, *ACS Nano* **2009**, *3*, 1767; b) W. Gaynor, G. F. Burkhard, M. D. McGehee, P. Peumans, *Adv. Mater.* **2011**, *23*, 2905; c) C.-H. Liu, X. Yu, *Nanoscale Res. Lett.* **2011**, *6*, 75.
- [39] a) J. Lee, I. Lee, T. S. Kim, J. Y. Lee, *Small* **2013**, *9*, 2887; b) G. Y. Margulis, M. G. Christoforo, D. Lam, Z. M. Bailey, A. R. Bowring, C. D. Bailie, A. Salleo, M. D. McGehee, *Adv. Energy Mater.* **2013**, *3*, 1657.
- [40] a) S. Das, A. Garg, A. I. Campbell, J. Howse, A. Sen, D. Velegol, R. Golestanian, S. J. Ebbens, *Nat. Commun.* **2015**, *6*, 8999; b) J. Katuri, D. Caballero, R. Voituriez, J. Samitier, S. Sanchez, *ACS Nano* **2018**, *12*, 7282; c) J. Simmchen, J. Katuri, W. E. Uspal, M. N. Popescu, M. Tasinkevych, S. Sanchez, *Nat. Commun.* **2016**, *7*, 10958.
- [41] M. D. Abràmoff, P. J. Magalhães, S. J. Ram, *Biophotonics Int.* **2004**, *11*, 36.